International Journal of Applied Power Engineering (IJAPE)
Vol. 15, No. 3, September 2026, pp. 1064~1071
ISSN: 2252-8792, DOI: 10.11591/ijape.v15.i3.pp1064-1071

Analysis of charge transport kinetics in photovoltaic based on FTO@TiO_2@CdS:Cu^{2+}@ZnS photoanode

Thai Van Thanh, Nguyen Van Minh, Ho Minh Trung
Vinh Long University of Technology Education, Vinh Long, Vietnam

Article Info

Article history:

Received Jul 29, 2025
Revised Mar 20, 2026
Accepted Jun 10, 2026

Keywords:

Charge recombination
High efficiency
Nanoscrystals
Quantum dots
Solar cell

ABSTRACT

This study examines charge-transport kinetics in TiO_2@CdS:Cu^{2+}@ZnS quantum dot–sensitized solar cells, addressing a key research gap regarding how controlled Cu^{2+} incorporation simultaneously affects recombination dynamics and interfacial charge-transfer resistances. While previous works mainly emphasized optical improvements from Cu doping, the coupled effects on impedance characteristics and device performance remain insufficiently clarified. Cu-doped CdS quantum dots with concentrations ranging from 0 to 0.5 mol were synthesized via the SILAR method and protected with a ZnS passivation layer. Electrochemical impedance spectroscopy and I–V characterization were employed to quantify changes in R_{ct1}, R_{ct2}, J_{sc}, V_{oc}, fill factor, and power conversion efficiency. The optimal Cu(0.2) device achieved 4.69% efficiency with a Jsc of 27.4 mA/cm², reflecting enhanced charge transport, reduced recombination, and improved light absorption. The findings reveal the previously underexplored dual role of Cu doping in tuning both optical and electronic properties. Furthermore, they identify the threshold at which excessive Cu leads to recombination-dominated losses and structural degradation. This work establishes a clearer mechanistic basis for engineering high-performance quantum absorber architectures in next-generation solar cell technologies.

Corresponding Author:

Nguyen Van Minh
Vinh Long University of Technology Education
Vinh Long, Vietnam
Email: minhnv@vlute.edu.vn

1. INTRODUCTION

Dye-sensitized solar cells (DSSCs) have been widely studied over recent decades, achieving efficiencies above 15% [1], [2]. However, further performance improvement is constrained by the Shockley–Queisser limit, largely due to thermalization losses and the narrow absorption range of organic dyes. Since 2000, quantum dot-sensitized solar cells (QDSSCs) have emerged as a promising alternative capable of surpassing this limit [3]-[6]. Nanocrystals, used in place of dyes, exhibit high size-dependent absorption coefficients, broad spectral absorption, and the ability to generate multiple excitons per absorbed photon. Materials such as CdS, CdSe, PbS, PbSe, and CdTe have been incorporated into photoanodes, though their efficiencies remain limited by the narrow absorption spectrum of individual quantum dots [7]-[11].

To address this challenge, researchers have developed multilayer quantum dot architectures using techniques such as successive ionic layer adsorption and reaction (SILAR) and chemical bath deposition (CBD), achieving notable increases in current density and overall efficiency [12]-[14]. Metal doping has further enhanced QDSSC performance, with reported efficiencies of 2.5% for Hg–PbS, 3.77% for Mn–CdS/CdSe, 4.22% for Cu–CdSe, and 2.72% for Ag–CdSe, primarily due to impurity levels introduced within the band gap [15]-[21]. However, prior studies have not simultaneously co-doped quantum dots such as CdS and CdSe, a strategy expected to broaden absorption spectra and significantly boost photocurrent.

I–V measurements alone provide limited mechanistic insight because they cannot independently resolve recombination, transport resistance, and series resistance contributions. A more complete understanding is obtained by combining I–V analysis with electrochemical impedance spectroscopy (EIS). Although QDSSCs share structural similarities with DSSCs, their distinct quantum dot layers, counter electrodes, and electrolytes require adapted EIS interpretation. Illuminated EIS spectra enable the deconvolution of resistance components associated with electron transport, recombination, and ion diffusion, while equivalent-circuit modeling yields key parameters essential for elucidating charge dynamics in QDSSC devices.

2. EXPERIMENTAL SECTION

The fabrication of the photoanode and counter electrode was carried out through a multi-step process designed to ensure high crystallinity, efficient charge transport, and stable interfacial contact within the QDSSC structure.

2.1. Preparation of FTO/TiO_2 substrates

Fluorine-doped tin oxide (FTO) glass substrates were first cleaned ultrasonically in successive ethanol, acetone, and deionized water baths to remove organic residues and surface contaminants. After cleaning, a commercial anatase TiO_2 paste with 20 nm particle size (Dyesol) was prepared for deposition. The paste was then applied onto the FTO surface by screen-printing, ensuring uniform film thickness and strong mechanical adhesion.

The printed films were gradually heated to remove organic binders. They were then sintered at 500 °C for 30 minutes in air. This high-temperature treatment enhances the crystallinity of TiO_2, promotes necking between nanoparticles, and improves electron mobility throughout the mesoporous TiO_2 network.

2.2. Deposition of Cu-Doped CdS quantum dots via SILAR

Cu-doped CdS layers (CdS:Cu(x) with x = 0–0.5, corresponding to the molar ratio Cu^{2+}/Cd^{2+}) were grown onto the TiO_2 surface using the successive ionic layer adsorption and reaction (SILAR) technique. Each SILAR cycle consisted of: Immersion of the TiO_2 film into a 0.1 M Cd^{2+} solution ($Cd(CH_3COO)_2 \cdot 2H_2O$ in ethanol) for 5 minutes to allow the adsorption of Cd^{2+} ions. Rinsing with ethanol to remove loosely bound ions. Immersion into a 0.1 M Cu^{2+} solution ($CuCl_2$ in ethanol/water 1:1) for 5 minutes to incorporate Cu^{2+} into the CdS lattice during the formation of doped QDs.

Doping with Cu^{2+} introduces intermediary electronic states that facilitate enhanced light harvesting and modify recombination pathways. After completing the Cd^{2+}/Cu^{2+} SILAR cycles, the films were treated in 0.1 M Na_2S at 60 °C, enabling the in-situ formation of CdS:Cu nanoparticles. The samples were subsequently dried at 120 °C to stabilize the quantum dot layer and remove remaining solvents.

2.3. Fabrication of FTO@TiO_2@CdS:Cu(0.3) photoanode

For the optimized doping level (x = 0.3), additional enhancement cycles were performed to improve quantum dot loading and dopant incorporation. The TiO_2 films coated with CdS:Cu were subjected to three additional SILAR cycles using: A mixed Cd^{2+}/Cu^{2+} precursor solution with a Cu^{2+}/Cd^{2+} ratio of 0.3, promoting homogenous doping throughout the QD layer. A Se^{2-} source solution to partially convert CdS to CdS_xSe_{1-x}, thereby extending visible-light absorption and improving band alignment. These repeated deposition cycles increase surface coverage, reduce inter-particle gaps, and enhance photogenerated charge carrier collection.

2.4. Deposition of ZnS passivation layer

To suppress surface traps and minimize interfacial recombination, a ZnS passivation shell was deposited onto the CdS:Cu(0.3) films. This was achieved via two SILAR cycles, each involving: Immersion in 0.1 M Zn^{2+} solution, allowing Zn^{2+} adsorption on the QD surface. Immersion in 0.1 M Na_2S, promoting the in-situ reaction to form a thin ZnS overlayer. ZnS, with its wide bandgap (~3.7 eV), acts as an insulating barrier that reduces parasitic electron recombination with the electrolyte while maintaining efficient hole extraction from the photoanode.

2.5. Preparation of the FTO/Cu_2S counter electrode

The counter electrode was fabricated on an FTO substrate by chemically depositing Cu_2S, a widely used catalyst in polysulfide QDSSCs due to its high conductivity and electrocatalytic activity. The electrode area was controlled to 0.25 cm^2 to match the active area of the photoanode. The Cu_2S layer facilitates the redox conversion of S^{2-}/S_x^{2-} species in the electrolyte, enabling effective hole transport and completing the electrical circuit of the cell.

2.6. Assembly of the quantum dot–sensitized solar cells

The QDSSC devices were assembled by sandwiching the FTO/TiO_2/CdS:Cu(0.3)/ZnS photoanode with the FTO/Cu_2S counter electrode using a defined spacer. A polysulfide electrolyte containing 0.5 M Na_2S, 0.2 M elemental sulfur (S), and 0.2 M KCl was then prepared for injection. Finally, the electrolyte was introduced into the cell through pre-drilled holes or by capillary injection to complete the assembly.

2.7. Photovoltaic testing

The assembled cells were exposed to simulated solar illumination of approximately 100 mW cm^{-2} (AM 1.5G equivalent). The current–voltage characteristics were measured to evaluate: short-circuit current density, open-circuit voltage, fill factor, and power conversion efficiency. These parameters collectively characterize the optoelectronic performance of the synthesized photoanode structures.

3. RESULTS AND DISCUSSION

Figure 1 illustrates a simplified equivalent circuit commonly used to model the behavior of a photovoltaic device or a light-dependent current source. In this representation, the light-generated current is denoted by I_L, which serves as the primary current source of the system. A shunt resistance, R_{SH}, is connected in parallel with the current source to account for leakage pathways within the device. This resistance models undesired current loss due to defects, impurities, or recombination mechanisms that allow charge carriers to bypass the external load. A low shunt resistance typically indicates high leakage currents and degraded device performance, whereas a high R_{SH} represents a well-isolated junction with minimal parasitic losses.

The voltage across the circuit and the current flowing through the external path are indicated by the labeled arrows. Together, these elements form a foundational model used to analyze the electrical characteristics, efficiency, and loss mechanisms of optoelectronic devices such as solar cells and photodetectors (Figure 1).

i. Open-circuit condition:

$$I_{ph} = I_d + I_{SH} \tag{1}$$

$$I_{ph} = I_o(e^{\alpha V_{OC}} - 1) + \frac{V_{OC}}{R_{SH}} \tag{2}$$

With $\alpha = \frac{q}{nkT}$.

ii. Short-circuit condition:

$$I_{ph} = I_d + I_{SH} + I_{SC} \tag{3}$$

$$I_{ph} = I_o(e^{\alpha I_{SC} R_S} - 1) + \frac{I_{SC} R_S}{R_{SH}} + I_{SC} \tag{4}$$

iii. Loaded condition:

$$I_{ph} = I_d + I_{SH} + I_L \tag{5}$$

$$I_{ph} = I_o\left(e^{\alpha(V_L + I_L R_S)} - 1\right) + \frac{V_L + I_L R_S}{R_{SH}} + I_L \tag{6}$$

At any two points (V_1,I_1) and (V_2,I_2) on the I-V curve, the voltage–current relation becomes:

$$V_1 = \frac{1}{\alpha} ln\left[\frac{R_{SH}(I_{ph} + I_o - I_1)}{R_{SH} I_o} - I_1 R_S\right] - I_1 R_S \tag{7}$$

$$V_2 = \frac{1}{\alpha} ln\left[\frac{R_{SH}(I_{ph} + I_o - I_2)}{R_{SH} I_o} - I_2 R_S\right] - I_2 R_S \tag{8}$$

Subtracting (7) and (8) yields the expression for R_S:

$$R_S = \frac{V_1 - V_2}{I_2 - I_1} - \frac{1}{\alpha(I_2 - I_1)} ln\left[\frac{R_{SH}(I_{ph} + I_o - I_1) - I_1 R_S}{R_{SH}(I_{ph} + I_o - I_2) - I_2 R_S}\right] \tag{9}$$

Since in practice $R_{SH} \gg R_S$, the approximations $R_{SH}(I_{ph} + I_o - I_1) \gg I_1 R_S$; $R_{SH}(I_{ph} + I_o - I_2) \gg I_2 R_S$: hold, simplifying (9) to

$$R_S = \frac{V_1 - V_2}{I_2 - I_1} - \frac{1}{\alpha(I_2 - I_1)} ln\left[\frac{I_{ph} + I_o - I_1}{I_{ph} + I_o - I_2}\right] = R_D - R_d \quad (10)$$

Where:

$$R_D = \frac{V_1 - V_2}{I_2 - I_1} \quad (11)$$

$$R_d = \frac{1}{\alpha(I_2 - I_1)} ln\left[\frac{I_{ph} + I_o - I_1}{I_{ph} + I_o - I_2}\right] \quad (12)$$

R_D and R_d represent the external and internal dynamic resistances of the photovoltaic module, respectively. The shunt resistance is obtained from the open-circuit expression:

$$R_{SH} = \frac{V_{OC}}{I_{ph} - I_o(e^{\alpha V_o} - 1)} \quad (13)$$

Additionally, R_S can be evaluated from the dark I–V curve:

$$R_S = -\frac{V_1 - V_2}{I_2 - I_1} + \frac{1}{\alpha(I_2 - I_1)} ln\left[\frac{I_o - I_1}{I_o - I_2}\right] = R_d - R_D \quad (14)$$

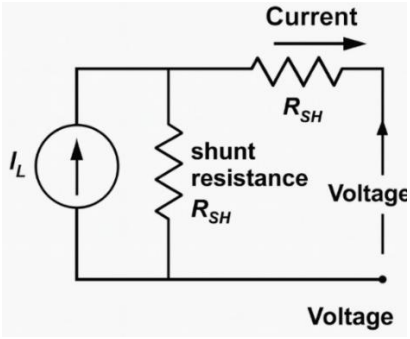

Figure 1. Schematic diagram of the QDSSC's equivalent circuit [22]

The formulas describe the current–voltage relationships in the diode model of a photovoltaic cell. For each operating condition—open circuit, short circuit, and loaded—the photocurrent, diode diffusion current, and shunt current must satisfy Kirchhoff's current law. The series resistance and shunt resistance are extracted by analyzing two arbitrary points on the I–V curve and separating the external dynamic resistance from the internal dynamic resistance. When RSH is very large (which is typical for many PV modules), the model simplifies because the shunt leakage current becomes negligible. Additionally, RS can also be determined from the dark I–V curve, where only the diode current is present, allowing for more accurate parameter modeling.

The TiO_2@CdS solar cells doped with varying Cu concentrations (0–0.5 mol) exhibit clear trends in key photovoltaic parameters (Voc, Jsc, FF, and PCE). Cu incorporation slightly increases Voc from 0.48 V (undoped) to 0.50 V for Cu ≥ 0.1, indicating reduced interfacial recombination (Figure 2). Jsc rises significantly from 19.9 to 27.35 mA/cm² at 0.2 mol Cu, followed by a decline at higher doping levels, suggesting that moderate Cu content enhances charge transport and light absorption, while excessive Cu introduces defects that promote recombination. The FF shows a similar behavior, peaking at 0.38 for Cu(0.1) and decreasing thereafter due to increased internal resistance. As a result, PCE reaches a maximum of 4.69% at Cu(0.2) before declining at higher Cu contents. These observations confirm that controlled Cu doping—optimally at 0.2 mol—enhances QDSSC performance, whereas overdoping degrades structural integrity and increases carrier recombination.

Dynamic resistance analysis based on a single illuminated I–V curve allows separation of the total resistance into external (R_D) and internal (R_d) components, following established QDSSC modeling methods

[22]-[25]. Resistance values calculated from (7)–(9) show strong dependence on QDs film thickness and Cu concentration. The undoped sample exhibits the highest interfacial resistance (I_O = 1.76×10⁻⁶ Ω·cm²) and correspondingly large R_D (66.7 Ω) and Rd (1850 Ω). Introducing 0.1 mol Cu sharply reduces IO but simultaneously increases R_D and R_d, indicating that while Cu improves surface charge transfer, it also perturbs internal charge pathways through Cu–QDs interactions.

For Cu concentrations of 0.2–0.3 mol, the resistance parameters (I_O, R_D, R_d) stabilize, and RS slightly decreases (2690–2710 Ω·cm²), reflecting optimized charge transport. Although I_O reaches its lowest value (8.4×10⁻⁸ Ω·cm²) at 0.5 mol Cu, both R_D and R_d increase substantially, revealing an overdoping effect that enhances electron–hole recombination and impedes carrier transport [26]-[29]. Notably, Cu(0.2) shows the highest R_{SH} (27.3 kΩ·cm²), indicating minimized leakage current and the most balanced resistance profile. Overall, TiO_2@CdS:Cu(0.2) achieves the optimal trade-off among recombination suppression, charge transport, and leakage minimization, yielding the best QDSSC device performance.

Compared with previously reported CdS-based QDSSCs, the Cu-doped samples in this study exhibit competitive or superior photovoltaic performance, particularly in terms of Jsc and PCE. The CdS:Cu(0.2) photoanode achieves a PCE of 4.69%, which surpasses many literature values typically ranging from 2–4% for undoped or singly doped CdS systems. Moreover, the remarkably low R_{ct2} (24.7 Ω) indicates more efficient charge transfer than most reported architectures, where interfacial resistances commonly exceed 50–200 Ω. Overall, our optimized Cu doping yields enhanced carrier transport and reduced recombination, demonstrating clear improvements over comparable studies. The detailed photovoltaic parameters obtained from the two-point extraction method and the solar-cell efficiency model are presented in Table 1.

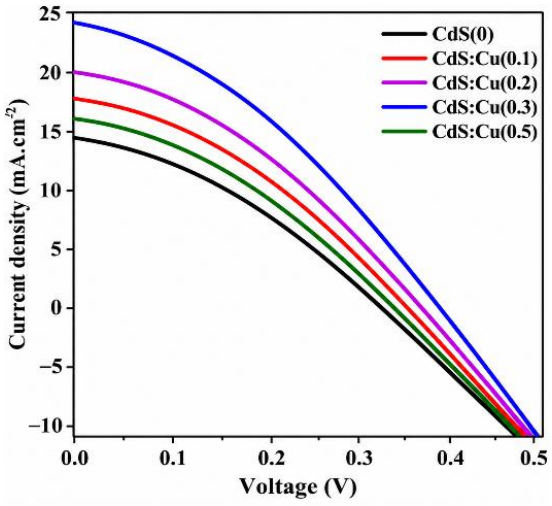

Figure 2. The power conversion efficiency of the QDSSCs

Table 1. Device parameters of the QDSSCs were evaluated using a two-point extraction method linked to the efficiency model of the solar cell

Samples	IO (Ω/cm2)	Rd (Ω)	RD (Ω)	RS (Ω.cm2)	RSH (kΩ.cm2)
CdS:Cu(0)	1.76.10-6	1850	66.7	1780	19.9
CdS:Cu(0.1)	8.9.10-8	3390	121.7	3270	21.9
CdS:Cu(0.2)	1.1.10-7	2790	100.3	2690	27.3
CdS:Cu(0.3)	9.6.10-8	2810	100	2710	23.7
CdS:Cu(0.5)	8.4.10-8	5410	200	5210	20.8

Electrochemical impedance spectroscopy was employed to analyze the kinetic processes of QDSSCs fabricated with five Cu-doped CdS nanocrystal concentrations. The experimental spectra were fitted to an equivalent circuit to extract R_{ct1} and R_{ct2}, corresponding to charge-transfer resistance at the Cu_2S/electrolyte interface and at the TiO_2/nanocrystal interface, respectively. As shown in Table 2 and Figure 3, lower resistance values correlate with reduced recombination and enhanced photocurrent. The device using FTO@TiO_2@CdS:Cu(0.3)@ZnS with 0.2 Cu doping exhibits the lowest resistances (R_{ct1} = 10.6 Ω, R_{ct2} = 24.7 Ω), indicating faster interfacial electron transport and suppressed recombination, consistent with the observed increase in Jsc to 27.4 mA·cm⁻². Moderate Cu doping improves light absorption and

electron generation/collection in agreement with the enhanced optical spectra reported by Nguyen *et al.* [18]. When the Cu concentration deviates from 0.2, both Rct1 and R_{ct2} increase—e.g., R_{ct2} rises to 186.5 Ω (0 Cu) and 143.2 Ω (0.1 Cu)—due to the inherently higher resistance of Cd relative to Cu in CdS and CdS:Cu^{2+} films. At higher Cu loadings, absorption and FESEM results reveal film non-uniformity and particle agglomeration, which impair charge transfer. These findings align with Muthalif *et al*. [30], who also observed improved light harvesting and efficiency upon Cu incorporation into CdS QDSSC photoanodes [30]-[34].

Table 2. Parameters used to characterize the QDSSCs

Samples	Voc (V)	Jsc (mA.cm-2)	FF	PCE (%)	Rct1 (Ω)	Rct2 (Ω)
CdS:Cu(0)	0.48	19.9	0.345	3.3	12	186.5
CdS:Cu(0.1)	0.501	21.9	0.38	3.96	11	143.2
CdS:Cu(0.2)	0.5011	27.4	0.35	4.69	10.5	24.7
CdS:Cu(0.3)	0.503	23.7	0.35	4.42	10.9	55.6
CdS:Cu(0.5)	0.5035	20.8	0.35	3.61	11.3	153.3

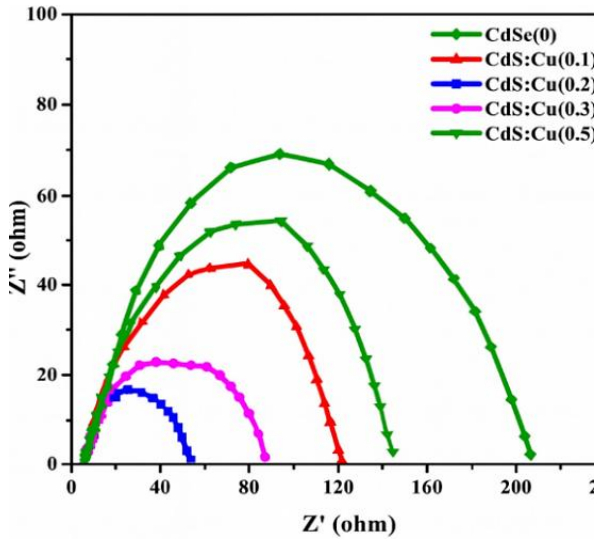

Figure 3. Electrochemical impedance response of the QDSSCs

4. CONCLUSION

Using TiO_2@CdS:Cu(x)@ZnS photoanodes (x = 0–0.5), we fabricated and systematically evaluated QDSSCs to elucidate the role of Cu^{2+} doping. The results demonstrate that Cu incorporation strongly influences internal/external resistances, charge-transport behavior, and overall device efficiency. The Cu(0.2) sample exhibited the most optimal photovoltaic response, achieving a PCE of 4.69%, Jsc of 27.4 mA/cm², and the lowest R_{ct1}/R_{ct2} values, attributed to enhanced light absorption, improved electron injection, and suppressed recombination. In contrast, excessive doping ($x \geq 0.3$) introduced structural defects, increased resistive losses, and reduced efficiency. EIS measurements corroborated these trends and provided detailed insights into charge-transfer kinetics. These findings underscore the necessity of precise Cu-doping control to optimize QDSSC performance and contribute to the rational design of high-efficiency nanostructured photoanodes for next-generation solar technologies.

FUNDING INFORMATION

Authors state no funding involved.

AUTHOR CONTRIBUTIONS STATEMENT

This journal uses the Contributor Roles Taxonomy (CRediT) to recognize individual author contributions, reduce authorship disputes, and facilitate collaboration.

Name of Author	C	M	So	Va	Fo	I	R	D	O	E	Vi	Su	P	Fu
Thai Van Thanh	✓	✓	✓	✓	✓	✓		✓	✓	✓			✓	
Nguyen Van Minh		✓				✓		✓	✓	✓	✓	✓		
Ho Minh Trung		✓				✓		✓	✓	✓	✓	✓		

C : **C**onceptualization
M : **M**ethodology
So : **So**ftware
Va : **Va**lidation
Fo : **Fo**rmal analysis
I : **I**nvestigation
R : **R**esources
D : **D**ata Curation
O : Writing - **O**riginal Draft
E : Writing - Review & **E**diting
Vi : **Vi**sualization
Su : **Su**pervision
P : **P**roject administration
Fu : **Fu**nding acquisition

CONFLICT OF INTEREST STATEMENT

Authors state no conflict of interest.

DATA AVAILABILITY

The data that support the findings of this study are available on request from the corresponding author, [NVM]. The data, which contain information that could compromise the privacy of research participants, are not publicly available due to certain restrictions.

REFERENCES

[1] Y. Hu *et al.*, "Incorporation of γ-aminobutyric acid and cesium cations to formamidinium lead halide perovskites for highly efficient solar cells," *Journal of Energy Chemistry*, vol. 64, pp. 561–567, 2021, doi: 10.1016/j.jechem.2021.05.025.

[2] D. Luo *et al.*, "Electron-deficient diketone unit engineering for non-fused ring acceptors enabling over 13% efficiency in organic solar cells," *Journal of Materials Chemistry A*, vol. 9, no. 26, pp. 14948–14957, 2021, doi: 10.1039/d1ta03643b.

[3] S. Rühle, M. Shalom, and A. Zaban, "Quantum-dot-sensitized solar cells," *ChemPhysChem*, vol. 11, no. 11, pp. 2290–2304, 2010.

[4] A. W. Cohn, A. M. Schimpf, C. E. Gunthardt, and D. R. Gamelin, "Size-dependent trap-assisted Auger recombination in semiconductor nanocrystals," *Nano Letters*, vol. 13, no. 4, pp. 1810–1815, 2013, doi: 10.1021/nl400503s.

[5] Y. Zhang, J. Liu, S. L. Li, Z. M. Su, and Y. Q. Lan, "Polyoxometalate-based materials for sustainable and clean energy conversion and storage," *EnergyChem*, vol. 1, no. 3, p. 100021, 2019, doi: 10.1016/j.enchem.2019.100021.

[6] J. Tian *et al.*, "Architectured ZnO photoelectrode for high efficiency quantum dot sensitized solar cells," *Energy and Environmental Science*, vol. 6, no. 12, pp. 3542–3547, 2013, doi: 10.1039/c3ee41056k.

[7] P. V. Kamat and J. H. Bang, "Quantum dot sensitized solar cells: tale of two semiconductor nanocrystals – CdSe and CdTe," *ACS National Meeting Book of Abstracts*, vol. 3, no. 6, pp. 1467–1476, 2009.

[8] V. González-Pedro *et al.*, "Ultrafast characterization of the electron injection from CdSe quantum dots and dye n719 co-sensitizers into TiO2 using sulfide-based ionic liquid for enhanced long-term stability," *Electrochimica Acta*, vol. 100, pp. 35–43, 2013, doi: 10.1016/j.electacta.2013.03.119.

[9] R. D. Schaller and V. I. Klimov, "High efficiency carrier multiplication in PbSe nanocrystals: implications for solar energy conversion," *Physical Review Letters*, vol. 92, no. 18, p. 186601, 2004, doi: 10.1103/PhysRevLett.92.186601.

[10] K. Hara, K. Sayama, Y. Ohga, A. Shinpo, S. Suga, and H. Arakawa, "A coumarin-derivative dye-sensitized nanocrystalline TiO2 solar cell having a high solar energy conversion efficiency up to 5.6 per cent," *Renewable Energy: Four Volume Set*, vol. 2–4, no. 6, pp. 214–218, 2018, doi: 10.4324/9781315793245-58.

[11] J. K. Sun, Y. Jiang, X. Zhong, J. S. Hu, and L. J. Wan, "Three-dimensional nanostructured electrodes for efficient quantum-dot-sensitized solar cells," *Nano Energy*, vol. 32, pp. 130–156, 2017, doi: 10.1016/j.nanoen.2016.12.022.

[12] S. A. Pawar, D. S. Patil, J. H. Kim, P. S. Patil, and J. C. Shin, "Quantum dot sensitized solar cell based on TiO2/CdS/Ag2S heterostructure," *Optical Materials*, vol. 66, pp. 644–650, 2017, doi: 10.1016/j.optmat.2017.03.011.

[13] Y. Zhang, J. Zhu, X. Yu, J. Wei, L. Hu, and S. Dai, "The optical and electrochemical properties of CdS/CdSe co-sensitized TiO2 solar cells prepared by successive ionic layer adsorption and reaction processes," *Solar Energy*, vol. 86, no. 3, pp. 964–971, 2012, doi: 10.1016/j.solener.2012.01.006.

[14] F. Huang *et al.*, "High efficiency CdS/CdSe quantum dot sensitized solar cells with two ZnSe layers," *ACS Applied Materials and Interfaces*, vol. 8, no. 50, pp. 34482–34489, 2016, doi: 10.1021/acsami.6b12842.

[15] I. Mora-Seró *et al.*, "Recombination in quantum dot sensitized solar cells," *Accounts of Chemical Research*, vol. 42, no. 11, pp. 1848–1857, 2009, doi: 10.1021/ar900134d.

[16] Q. Dai, E. M. Sabio, W. Wang, and J. Tang, "Pulsed laser deposition of Mn-doped CdSe quantum dots for improved solar cell performance," *Applied Physics Letters*, vol. 104, no. 18, 2014, doi: 10.1063/1.4875107.

[17] N. T. Thao, H. N. Phuong, H. T. Tung, N. T. Phat, H. T. Dat, and L. Q. Vinh, "The enhanced current density of the quantum dots solar cells based on CdSe: Mn2+ crystalline," *Optical Materials*, vol. 84, pp. 199–204, 2018, doi: 10.1016/j.optmat.2018.06.069.

[18] T. P. Nguyen, T. T. Ha, T. T. Nguyen, N. P. Ho, T. D. Huynh, and Q. V. Lam, "Effect of Cu2+ ions doped on the photovoltaic features of CdSe quantum dot sensitized solar cells," *Electrochimica Acta*, vol. 282, pp. 16–23, 2018, doi: 10.1016/j.electacta.2018.06.046.

[19] J. Yang, S. Mei, and J. M. Ferreira, "Hydrothermal synthesis of well-dispersed tio$_2$ nano-crystals," *Journal of Materials Research*, vol. 17, no. 9, pp. 2197–2200, 2002.

[20] S. Hachiya, Q. Shen, and T. Toyoda, "Effect of ZnS coatings on the enhancement of the photovoltaic properties of PbS quantum dot-sensitized solar cells," *Journal of Applied Physics*, vol. 111, no. 10, 2012, doi: 10.1063/1.4720468.

[21] J. Ebothé, J. Michel, I. V. Kityk, G. Lakshminarayana, O. M. Yanchuk, and O. V. Marchuk, "Influence of CdS nanoparticles grain morphology on laser-induced absorption," *Physica E: Low-Dimensional Systems and Nanostructures*, vol. 100, pp. 69–72, 2018, doi: 10.1016/j.physe.2018.03.002.

[22] T. Ha Thanh, V. Lam Quang, and D. Huynh Thanh, "Determination of the dynamic resistance of the quantum dots solar cells by one I-V curve and electrochemical impedance spectra," *Solar Energy Materials and Solar Cells*, vol. 143, pp. 269–274, 2015, doi: 10.1016/j.solmat.2015.07.007.
[23] C. Li *et al.*, "ZnO nanoparticle-based highly efficient CdS/CdSe quantum dot-sensitized solar cells," *Physical Chemistry Chemical Physics*, vol. 15, no. 22, pp. 8710–8715, 2013, doi: 10.1039/c3cp50365h.
[24] Y. J. Hsu and S. Y. Lu, "One-step preparation of coaxial CdS-ZnS nanowires," *Chemical Communications*, vol. 15, no. 18, pp. 2102–2103, 2004, doi: 10.1039/b403932g.
[25] V. I. Klimov *et al.*, "Optical gain and stimulated emission in nanocrystal quantum dots," *Science*, vol. 290, no. 5490, pp. 314–317, 2000, doi: 10.1126/science.290.5490.314.
[26] A. Roy, M. J. S. Mohamed, M. A. Gondal, T. K. Mallick, A. A. Tahir, and S. Sundaram, "Co-sensitization effect of N719 dye with Cu doped CdS colloidal nanoparticles for dye sensitized solar cells," *Inorganic Chemistry Communications*, vol. 148, p. 110298, 2023, doi: 10.1016/j.inoche.2022.110298.
[27] D. J. Tarimo, K. O. Oyedotun, A. Mirghin, N. F. Sylla, and N. Manyala, "Asymmetric ultracapacitor produced by sulphur reduced graphene oxide/metal oxide composite with high energy density and outstanding cycling," in *ECS Meeting Abstracts*, The Electrochemical Society, Inc., 2022, pp. 69–69, doi: 10.1149/ma2022-02169mtgabs.
[28] J. Hou *et al.*, "High performance of Mn-doped CdSe quantum dot sensitized solar cells based on the vertical ZnO nanorod arrays," *Journal of Power Sources*, vol. 325, pp. 438–445, 2016, doi: 10.1016/j.jpowsour.2016.06.070.
[29] C. Zhang, S. Liu, X. Liu, F. Deng, Y. Xiong, and F. C. Tsai, "Incorporation of Mn2+ into CdSe quantum dots by chemical bath co-deposition method for photovoltaic enhancement of quantum dot-sensitized solar cells," *Royal Society Open Science*, vol. 5, no. 3, p. 171712, 2018, doi: 10.1098/rsos.171712.
[30] M. P. A. Muthalif, Y. S. Lee, C. D. Sunesh, H. J. Kim, and Y. Choe, "Enhanced photovoltaic performance of quantum dot-sensitized solar cells with a progressive reduction of recombination using Cu-doped CdS quantum dots," *Applied Surface Science*, vol. 396, pp. 582–589, 2017, doi: 10.1016/j.apsusc.2016.10.200.
[31] Z. Li, L. Yu, Y. Liu, and S. Sun, "Efficient quantum dot-sensitized solar cell based on cdsxse1-x/mn-cds/Mn-CdS/TiO2 nanotube array electrode," *Electrochimica Acta*, vol. 153, pp. 140–148, 2015, doi: 10.1016/j.electacta.2014.11.197.
[32] T. H. Thanh, Q. V. Lam, T. H. Nguyen, and T. D. Huynh, "Performance of CdS/CdSe/ZnS quantum dot-sensitized TiO_2 mesopores for solar cells," *Chinese Optics Letters*, vol. 11, no. 7, pp. 072501–072504, 2013, doi: 10.3788/col201311.072501.
[33] Y. S. Chang, M. Choi, M. Baek, P. Y. Hsieh, K. Yong, and Y. J. Hsu, "CdS/CdSe co-sensitized brookite h: TiO2 nanostructures: charge carrier dynamics and photoelectrochemical hydrogen generation," *Applied Catalysis B: Environmental*, vol. 225, pp. 379–385, 2018, doi: 10.1016/j.apcatb.2017.11.063.
[34] Y. S. Chang, P. Y. Hsieh, T. F. Mark Chang, C. Y. Chen, M. Sone, and Y. J. Hsu, "Incorporating graphene quantum dots to enhance the photoactivity of CdSe-sensitized TiO2 nanorods for solar hydrogen production," *Journal of Materials Chemistry A*, vol. 8, no. 28, pp. 13971–13979, 2020, doi: 10.1039/d0ta02359k.

BIOGRAPHIES OF AUTHORS

Thai Van Thanh obtained a master's degree in physics from Vinh University, Nghe An, Vietnam. He is currently teaching at the Faculty of Electrical and Electronic Engineering Technology, Vinh Long University of Technology Education. He focuses on the development of material technologies, semiconductors, and related fields. He can be contacted at email: thanhtv@vlute.edu.vn.

Nguyen Van Minh holds a Ph.D. in electrical engineering from Hanoi University of Science and Technology. He is currently the head of training and quality assurance, teaching undergraduate programs in electrical and electronic engineering technology and automation. He also teaches master's programs in electrical engineering and supervises postgraduate students in electrical engineering. His research focuses on: power quality, electrical energy, renewable energy, power system parameter optimization, smart grids, distributed power, and electrical equipment control. He can be contacted at email: minhnv@vlute.edu.vn.

Ho Minh Trung received the Ph.D. degree in physics from University of Science, Vietnam National University Ho Chi Minh City, Vietnam. He is working as a lecturer at the Faculty of Basic Sciences, Vinh Long University of Technology Education, Vietnam. His research interests focus on developing the patterned substrate with micro- and nano-scale to apply for physical and chemical devices such as solar cells, OLED, and photoanode. He can be contacted at email: trunghm@vlute.edu.vn.